A Continuous Process for Structurally Well-Defined Al$_2$O$_3$ Nanotubes Based on Pulse Anodization of Aluminum

Woo Lee,[*,†,‡] **Roland Scholz,**[†] **and Ulrich Gösele**[†]

Max Planck Institute of Microstructure Physics, Weinberg 2, D-06120 Halle, Germany and Korea Research Institute of Standards and Science (KRISS), Yuseong, 305-340 Daejon, Korea

ABSTRACT

A continuous process for the preparation of structurally well-defined uniform alumina (Al$_2$O$_3$) nanotubes was developed. The present nanofabrication approach is based on pulse anodization of aluminum by using sulfuric acid and provides unique opportunity for a facile tailoring of the length of nanotubes by controlling the pulse duration.

Nanotubes have many desirable characteristics based on their shape, potential quantum-size effects and a large effective surface area and thus have attracted considerable research interest.[1,2] Particular attention has been paid to the preparation of metal oxide nanotubes because of their potential applications in advanced electronics and for high performance catalysts. To date, various synthetic methods have been developed for oxide nanotubes of aluminum, iron, vanadium, titanium, silicon, zirconium, etc.[1–3] Among them, alumina nanotubes have a special importance for nanoelectronics and catalysis because of the material's excellent physicochemical properties, including high dielectric constant, very low permeability, high thermal conductivity, and chemical inertness.[4–6] Previously, alumina nanotubes have been prepared by wet-chemical etching of a porous alumina membrane,[7] by anodization of Al/Si,[8] or by utilizing one-dimensional organic or inorganic nanowires as sacrificial templates in hydrothermal synthesis,[9,10] a sol−gel technique,[11] chemical vapor deposition (CVD),[12] or atomic layer deposition (ALD).[13,14] However, apart from processing time, these methods have inherent disadvantages in fabricating alumina nanotubes with uniform diameter and in tailoring the length of nanotubes simultaneously. In this letter, we report a novel continuous method for the preparation of structurally well-defined alumina nanotubes with controllable length. The approach is based on pulse anodization of aluminum, combining both mild (MA) and hard anodization (HA) conditions, where the pulse duration defines the length of

alumina nanotubes. Previously MA has popularly been employed in nanotechnology research, because it enables the preparation of self-ordered anodic aluminum oxide (AAO) in spite of its limited processing windows (i.e., the so-called self-ordering regimes) for ordered arrays of alumina nanopores. On the other hand, HA that is performed at relatively low temperatures and high current density (typically, $j > 50$ mA cm^{-2}) by using H$_2$SO$_4$ has routinely been utilized for various industrial applications by taking advantage of the high-speed growth ($50 - 100$ μm h^{-1}) of anodic films with high technical quality. However, pores of the resulting anodic films are less ordered than those produced by MA processes, and thus HA processes have been out of focus in academic research. On the other hand, pulse anodization has been employed in the aluminum industry since the early 1960s in an attempt to avoid burning problems (i.e., local thickening of oxide film with black spots due to catastrophic flow of electrical current at the barrier layer) associated with HA of aluminum and its alloys and thus to produce anodic films that are superior in hardness, corrosion resistance, and thickness uniformity at an efficient rate of production in comparison with the conventional HA methods.[15–18] However, the process has not been employed in current nanotechnology due to the nonuniform and disordered pore structure of the resulting anodic alumina, although we have recently demonstrated that pulse anodization can successfully be implemented to develop novel three-dimensional (3D) porous architectures.[19]

For HA at potentiostatic conditions, the current density (j) decreases exponentially as a function of time (t) after an initial sharp surge,[20,21] unlike conventional MA processes where the current density (j) is maintained at a steady-state

---

* To whom correspondence should be addressed. E-mail: woolee@kriss.re.kr. Fax: +82-42-868-5032.
† Max Planck Institute of Microstructure Physics.
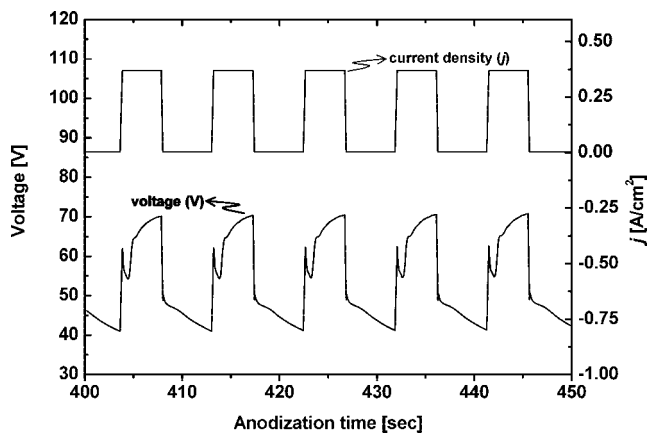‡ Korea Research Institute of Standards and Science (KRISS).

Figure 1. A typical current (j)-voltage relation during pulse anodization of aluminum. Pulses consist of MA-pulse ($j_{MA} = 3.16$ mA cm^{-2} and $\tau_{MA} = 5$ s) followed by HA-pulse ($j_{HA} = 368.42$ mA cm^{-2} and $\tau_{HA} = 4$ s).

value throughout the anodization. The growth rate of anodic oxide films in potentiostatic HA processes decreases with anodization time.[20,22] Therefore, we employed galvanostatic pulses for a better control of the tube length, since constant current ensures the constant growth rate of AAO. Periodic galvanic pulses consisting of a low current pulse followed by a high current pulse were applied in order to achieve MA and HA conditions, respectively. Pulse anodizations were conducted by using as-prepared 0.3 M H$_2$SO$_4$ without any pretreatment of the solution or addition of Al$_2$(SO$_4$)$_3$ into the solution that was employed by Chu et al.[23] for the former and by Zhao et al.[24] for the latter in an attempt to suppress "breakdown (or burning)" of the AAO film under a high current density, j (i.e., high electric field, E).

Figure 1 shows a representative current−voltage relation during pulse anodization of aluminum. The pulses consist of a HA-pulse ($j_{HA} = 368.42$ mA/cm^2 and $\tau_{HA} = 4$ s) followed by a MA-pulse ($j_{MA} = 3.16$ mA/cm^2 and $\tau_{MA} = 5$ s). A typical recovery effect[25,26] was observed for HA-pulses, where the voltage (U) increases steeply for a short period of time, passes through a relative maximum, then hits a minimum value after capacitive decay due to the barrier oxide layer formed by the previous pulse (i.e., RC-decay with $U \approx U_o\exp(-t/R_bC_b)$, where R_b and C_b are the resistance and the capacitance of the barrier layer, respectively), and finally increases gradually. On the other hand, only capacitive decay of the voltage (U) was observed for MA-pulses of 5 s duration. This is due to the thick barrier oxide layer (i.e., higher R_b and C_b) formed by the previous HA-pulse and thus to the relatively short pulse duration for voltage recovery. Therefore, we can ignore the contribution of MA-pulses to the formation of anodic oxide (i.e., MA−AAO segments) under the present condition with a relatively short MA-pulse duration. The recovery effect could be observed for MA-pulses also, when the pulse duration (τ_{MA}) was sufficiently long (Supporting Information, Figure S1).

The reaction involved in anodic oxidation of aluminum is exothermic. The dissolution of the resulting oxide by acid electrolyte is endothermic. However, the main contribu-

tion to heat generation in anodization of aluminum is related to current flow through the barrier oxide layer. The production of Joule's heat (Q) is proportional to the square of the current density (j) according to the following equation; $Q = Ujt = R_bj^2t$.[27] HA is accompanied by a large evolution of heat due to the high anodic current (j) associated with the high electric field (E) at the barrier oxide. The excessive heat does not only trigger burning or breakdown of an anodic film but promotes undesired acidic dissolution of the oxide membrane by the electrolyte. It is worth mentioning that pulse anodization promises effective dissipation of reaction heat, which is one of the major causes of burning of an anodic film during anodization of aluminum under high current density (j). The accumulated Joule's heat during a HA-pulse of a high current density can be efficiently dispersed during the subsequent MA-pulse of a low current density, overcoming "burning" of an anodic film.

After pulse anodizations at different pulse parameters ($\tau_{HA} = 2$, 4, and 6 s at $j_{HA} = 368.42$ mA cm^{-2} for HA-pulses; $\tau_{MA} = 5$ s at $j_{MA} = 3.16$ mA cm^{-2} for MA-pulses), free-standing AAOs were obtained by removing the underlying aluminum substrate by using a mixture solution of 0.2 M CuCl$_2$ and 6.1 M HCl. Representative electron micrographs of the resulting samples are shown in Figure 2 (Figure 2a−c for $\tau_{HA} = 2$ s, Figure 2d−f for $\tau_{HA} = 6$ s; see Supporting Information, Figure S2 for $\tau_{HA} = 4$ s). Cross-sectional SEM micrographs show clearly a series of horizontal lines with a periodic spacing, as indicated by white triangles (Figure 2a,d). These lines correspond to the interfaces of HA−AAO segments, and the spacing between lines to their lengths. As evident from the micrographs, the pulse duration (τ_{HA}) of HA determines the length of HA−AAO segments. Alumina nanotubes could be obtained by immersing an as-prepared sample into 0.2 M CuCl$_2$/6.1 M HCl solution (45 °C) for 20 min, followed by gentle ultrasonic treatment to release individual tubes from the AAO film. We found that CuCl$_2$/HCl solution facilitate homogeneous separation of alumina nanotubes. Sonication alone turned out to be insufficient to separate individual alumina nanotubes, although the junction strength between cells of hard anodized AAO segments is fairly weak. We assume that CuCl$_2$/HCl solution weakens further the junction strength between cells by chemically dissolving oxide material at the cell boundaries. This assumption is somewhat in line with the recent experimental observation by Zhao et al., who reported that triple junction points in AAO membrane formed by high current density ($j = 160$ mA/cm^2) anodization can preferentially be etched by aqueous CuCl$_2$/HCl solution due to the presence of some hydrated aluminum oxide (e.g., Al(OH)$_3$ or AlOOH) at the triple cell junction sites.[24] SEM micrographs of alumina nanotubes formed at different HA-pulse durations are shown in Figure 2b,e, demonstrating convenient and reliable control over the length of alumina nanotubes by varying the pulse duration of HA (i.e., τ_{HA}). TEM investigations of the resulting alumina nanotubes revealed continuous and uniform tube walls (Figure 2c,f). The average inner and outer diameter of the nanotubes was estimated to be 80 and 95 nm, respectively. It is expected that the inner diameter of alumina
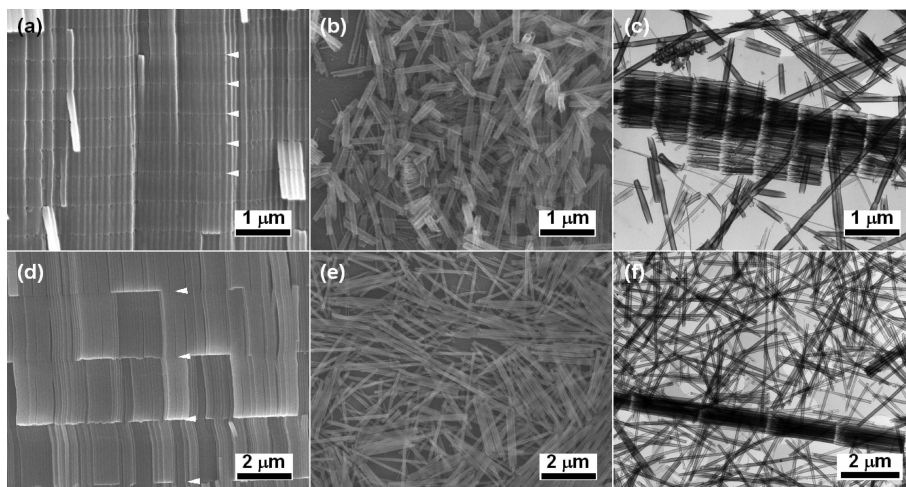
Figure 2. (a,d) Cross-sectional SEM micrographs of AAOs prepared by pulse anodization, showing the effect of HA-pulse duration on the tube length; (a) $\tau_{HA} = 2$ s and (d) $\tau_{HA} = 6$ s. Other pulse parameters were fixed at $j_{HA} = 368.42$ mA cm^{-2}, $j_{MA} = 3.16$ mA cm^{-2}, and $\tau_{MA} = 5$ s. (b,e) SEM micrographs of alumina nanotubes obtained from the samples shown in panels a,d, respectively; (b) $\tau_{HA} = 2$ s and (e) $\tau_{HA} = 6$ s. TEM micrographs of the corresponding samples are shown in panels c and f, respectively.
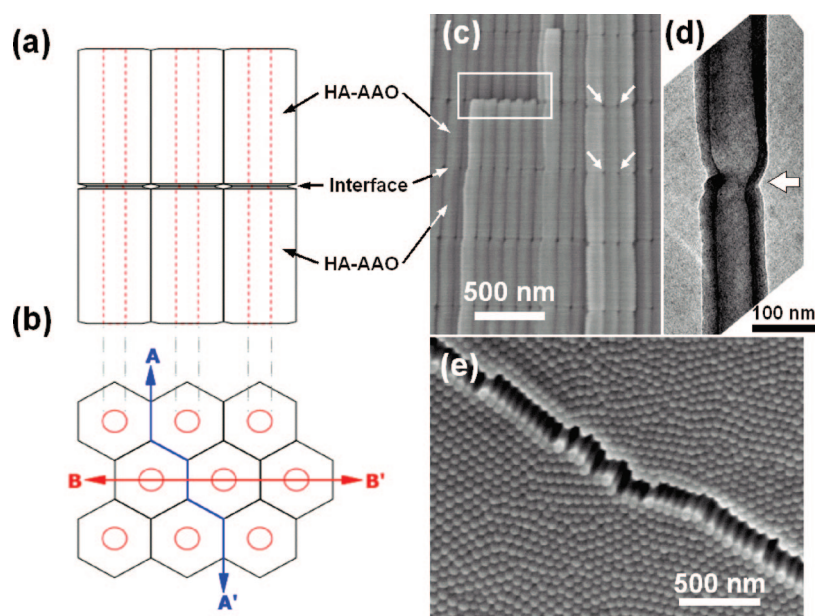

Figure 3. Schematics illustrating (a) cross-section of pulse anodized AAO, (b) two different fracture modes of AAOs (A−A′ cleavage plane for HA−AAO and B−B′ cleavage plane for MA−AAO). (c) A representative cross-sectional SEM micrograph of pulse anodized AAO ($j_{MA} = 3.16$ mA cm^{-2} and $\tau_{MA} = 10$ s for MA-pulses, $j_{HA} = 200$ mA cm^{-2} and $\tau_{HA} = 2$ s for HA-pulses). Horizontal fragmentation of AAO at the interfaces of HA−AAO segments is marked by a white rectangle in (c). White arrows in (c) indicate voids around the interface of HA−AAO segments. (d) TEM micrograph of a single alumina nanotube, showing a modulated pore structure. (e) Plane-view SEM micrograph of bottom surface of HA−AAO, manifesting crack propagation along cell boundaries (i.e., A-A′ cleavage plane in panel b).

nanotubes can be controlled by varying the etching time of pore walls by using an appropriate etching solution (e.g., H$_3$PO$_4$) prior to CuCl$_2$/HCl treatment. The formation of alumina nanotubes can be understood by considering the unique structural characteristics of AAOs formed by pulse anodization, as will be discussed below.

Upon closer examination of cross-sectional SEM micrographs of pulse anodized AAO (Figure 3c), one may see small voids around each interface of HA−AAO segments (see white arrows in Figure 3c). As highlighted by a white rectangle in Figure 3c, the junction strength between HA−AAO segments appears to be weak, resulting in horizontal fragmentation of AAO by weak external shear forces. This is one of the advantageous structural features of the samples formed by pulse anodization, enabling preparation of alumina nanotubes with controlled tube lengths. It is worth mentioning here that periodic galvanic pulses consisting of a low current pulse (j_{MA}) followed by a high current pulse (j_{HA}) give rise to periodic modulations of the pore diameter and the cell size of AAO. The pore
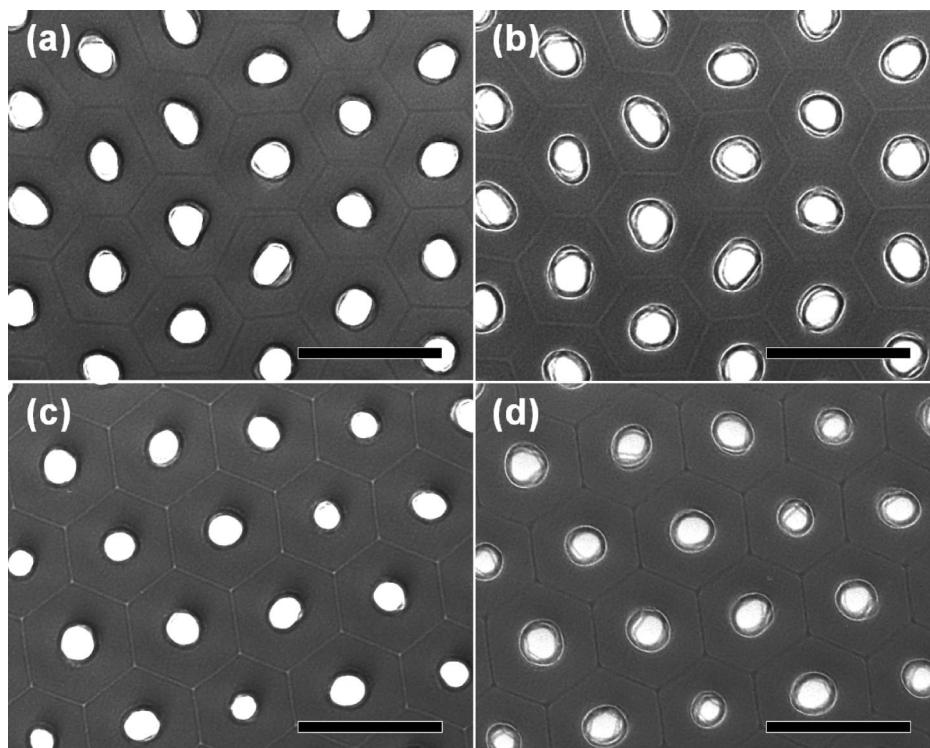
Figure 4. Plane-view TEM micrographs of (a,b) as-prepared mild- (MA) and (c,d) hard-anodized (HA) anodic aluminum oxide (AAO) under different focusing modes; panels a,c underfocus conditions and panels b,d overfocus conditions, manifesting the presence of voids at the cell boundaries of HA−AAO (scale bars = 100 nm).

diameter and the cell size of AAO at the interface of two HA−AAO segments was found to be smaller than that of HA−AAOs, as indicated by a white arrow in Figure 3d. Since MA-pulses do not contribute to the formation of AAO under the present pulsing condition (*vide supra*), we attribute the observed structural evolution solely to the HA-pulses. We believe that the voltage recovery during the period of a HA-pulse (j_{HA} = 368.42 mA cm^{-2}) is mainly responsible for this phenomenon. The average difference in voltage (*U*) measured at the early stage and at the end of a HA-pulse was found to be 15 V. Recent studies showed that the cell size of AAOs formed under HA conditions (i.e., high current density, *j*, or high electric field, *E*) increases with the formation voltage (*U*) at the rate of ζ_{HA} = 1.8 − 2.0 nm V^{-1},[20–23,28] that is lower than that (ζ_{MA} = 2.5 nm V^{-1}) for AAOs formed under conventional MA conditions.[29–31] Accordingly, we can estimate a maximum 30 nm of variation in the cell size during a voltage recovery, which results in periodic modulations of the pore structure during pulse anodization. We suggest that this unique structural feature in pulse anodized AAOs is mainly responsible for the weak junction strength between HA−AAO segments. However, we cannot completely rule out the contribution of tensile stress at the interfaces of HA−AAO segments to the weakening of the junction strength. Previous studies reported that the volume expansion factor involved in the oxidation of aluminum into alumina increases with electric field strength (*E*) across the barrier layer (i.e., current density, *j*).[32,33] We assume that a sharp transition of mechanical stress by periodic pulses might develop tensile stress at the

interfaces of HA−AAO segments, resulting in horizontal fragmentation of AAO by weak external stress.

It is also clear, from the SEM micrograph shown in Figure 3c, that the junction strength between cells of HA−AAO segments is fairly week, exhibiting an interesting fracture behavior along the vertical direction of the AAO against external stresses. Cracks propagate along the cell boundaries (i.e., the cleavage plane A−A′ in Figure 3b; also, see Figure 3e), rather than through the center of pores from pore to pore as in AAOs formed under conventional MA conditions using H$_2$SO$_4$, H$_2$C$_2$O$_4$, or H$_3$PO$_4$ electrolyte (i.e., the cleavage plane B−B′ in Figure 3b). Cleavage through the cell boundaries in HA−AAO segments resulted even in single Al$_2$O$_3$ nanotubes or bundles of tubes (so-called "Keller−Hunter−Robinson cells").[30,34] It was found, from our control experiments (not presented in detail here), that the junction strength between cells of HA−AAOs changes with the applied current density, *j* (i.e., electric field strength, *E*); the higher the applied current density, the weaker the junction strength between cells. This observation is in line with the recent result by Chu et al.[23] In 1986, Arrowsmith et al. and Wada et al. discussed for the first time the fracture behavior of AAOs formed under HA-conditions.[34,35] Recently Chu et al. suggested that weak junction strength of cells for AAOs formed by high-field anodization (i.e., HA−AAOs) is responsible for preferred cleavage along the cell boundaries.[23] They attributed the fracture along the cell boundaries in HA−AAO to the high level of interacting repulsive force concentrated at the boundaries of alumina cells, which is produced from volume expansion during oxide growth.[23]

However, compressive stress alone cannot reasonably account for the weak junction strength.

In order to reveal the origin of weak junction strength of cells in HA−AAO, we performed extensive TEM investigations on the samples prepared under MA- and HA-conditions. It has been well established that subnanometer sized cavities (or voids), that can hardly observe in-focus because of weak contrast in TEM observation, can be visualized by viewing them under defocus conditions by virtue of Fresnel diffraction effects.[36,37] An electron beam passing through a region containing nanometer-sized voids (or cavities) in an ultrathin specimen undergoes less phase retardation than electrons passing through void-free surrounding matrix.[38] The resulting phase shift causes an effective deflection of the electron beam which gives rise to an image contrast when the specimen is investigated under defocus conditions. For the overfocused condition (i.e., e-beam focused below the plane of the specimen), the contrast appears as a decreased image intensity at the center of a void, and as increased at the periphery of the void. For the underfocused condition (i.e., e-beam focused above the plane of the specimen), the contrast is opposite.

Plane-view TEM micrographs of as-prepared MA− and HA−AAO under different focusing conditions (i.e., underfocus and overfocus) are shown in Figure 4. Bright and dark image contrast at the peripheries of the primary pores at the center of each cell indicate defocusing conditions of the TEM; overfocus for the former and underfocus for the latter. In contrast to the case of MA−AAO (Figure 4a,b), bright image contrast at underfocus (Figure 4c) and reverse dark contrast at overfocus (Figure 4d) are evident along the cell boundaries of HA−AAO, manifesting the presence of free volume (i.e., voids) in these areas. It is believed that numerous nanometer-sized voids in the cell boundaries appear to be superimposed, giving continuous image contrasts. The formation mechanism of voids along the cell boundaries is not clear at the moment, but could be related to the evolution of oxygen gas bubbles from the anode surface during hard anodization of aluminum, which is mainly due to the oxidation of O^{2-} ions of the anodic oxide at the metal/oxide interface (i.e., $O^{2-} \rightarrow 1/2O_2 + 2e^-$).[39,40] We assume that the formation of voids along the cell boundaries during HA might be the origin of weak junction strength of the cells, leading to cracking of AAO along the cell boundaries. A discussion of cracking behavior of HA−AAO will be provided elsewhere.

In summary, a convenient method for the preparation of structurally well-defined alumina nanotubes with controllable length was developed. The approach is based on pulse anodization of aluminum. Periodic galvanic pulses were employed to achieve mild (MA) and hard anodization (HA) conditions, where the pulse duration for HA determines the length of nanotubes. By deliberately choosing the pulse parameters, not only were we able to achieve continuous tailoring of the pore structure of the resulting nanoporous anodic alumina (i.e., periodic modulation of pore diameters along the pore axis), but we were also able to weaken the junction strength between cells.

We could successfully separate individual alumina nanotubes from an as-prepared porous anodic alumina by taking advantage of the weak junction strength between cells and of the modulated pore structures along the pore axis. The generic capability of tailoring the length of alumina nanotubes in a well-controlled manner could make the present method attractive for developing nanotube-based functional nanostructures.

Supporting Information Available: Experimental details on pulse anodization of aluminum. Current−voltage relation curves, showing the recovery effect for mild anodization pulses with a long pulse duration. SEM micrograph of AAO formed by pulse anodization ($j_{MA} = 3.16$ mA cm^{-2}, $\tau_{MA} = 5$ s, $j_{HA} = 368.42$ mA cm^{-2}, $\tau_{HA} = 4$ s) and TEM micrograph of alumina nanotubes obtained from the corresponding sample. This material is available free of charge via the Internet at http://pubs.acs.org.

References
(1) Patzke, G. R.; Krumeich, F.; Nesper, R. *Angew. Chem., Int. Ed.* **2002**, *41*, 2446.
(2) Remškar, M. *Adv. Mater.* **2004**, *16*, 1497.
(3) Macák, J. M.; Tsuchiya, H.; Taveira, L.; Aldabergerova, S.; Schmuki, P. *Angew. Chem., Int. Ed.* **2005**, *44*, 7463.
(4) Gusev, E. P.; Copel, M.; Cartier, E.; Baumvol, I. J. R.; Krug, C.; Gribelyuk, M. A. *Appl. Phys. Lett.* **2000**, *76*, 176.
(5) Jongsomjit, B.; Panpranot, J.; James, G.; Goodwin, J. *J. Catal.* **2001**, *204*, 8.
(6) Peercy, P. S. *Nature* **2000**, *406*, 1023.
(7) Xiao, Z. L.; Han, C. Y.; Welp, U.; Wang, H. H.; Kwok, W. K.; Willing, G. A.; Hiller, J. M.; Cook, R. E.; Miller, D. J.; Crabtree, G. W. *Nano Lett.* **2002**, *2*, 1293.
(8) Pu, L.; Bao, X.; Zou, J.; Feng, D. *Angew. Chem., Int. Ed.* **2001**, *40*, 1490.
(9) Qu, L.; He, C.; Yang, Y.; He, Y.; Liu, Z. *Mater. Lett.* **2005**, *59*, 4034.
(10) Tang, B.; Ge, J.; Zhuo, L.; Wang, G.; Niu, J.; Shi, Z.; Dong, A. Y. *Eur. J. Inorg. Chem.* **2005**, *21*, 4366.
(11) Peng, T.; Yang, H.; Dai, K.; Nakanishi, K.; Hirao, K. *Adv. Eng. Mater.* **2004**, *6*, 241.
(12) Zhang, Y.; Liu, J.; He, R.; Zhang, Q.; Zhang, X.; Zhu, J. *Chem. Phys. Lett.* **2002**, *360*, 579.
(13) Hwang, J.; Min, B.; Lee, J. S.; Keem, K.; Cho, K.; Sung, M.-Y.; Lee, M.-S.; Kim, S. *Adv. Mater.* **2004**, *16*, 422.
(14) Wang, C.-C.; Kei, C.-C.; Yu, Y.-W.; Perng, T.-P. *Nano Lett.* **2007**, *7*, 1566.
(15) Kanagaraj, D.; Vincent, S.; Narasimhan, V. L. *Bull. Electrochem.* **1989**, *5*, 513.
(16) Miller, M. A. U.S. Patent 2,920,018, 1960.
(17) Raj, V.; Rajaram, M. P.; Balasubramanian, G.; Vincent, S.; Kanagaraj, D. *Trans. Inst. Met Finish.* **2003**, *81*, 114.
(18) Yokoyama, K.; Konno, H.; Takahashi, H.; Nagayama, M. *Plat. Surf. Finish.* **1982**, *69*, 62.
(19) Lee, W.; Schwirn, K.; Steinhart, M.; Pippel, E.; Scholz, R.; Gösele, U. *Nature Nanotech.* **2008**, *3*, 234.
(20) Lee, W.; Ji, R.; Gösele, U.; Nielsch, K. *Nat. Mater.* **2006**, *5*, 741.
(21) Schwirn, K.; Lee, W.; Hillebrand, R.; Steinhart, M.; Nielsch, K.; Gösele, U. *ACS Nano* **2008**, *2*, 302.
(22) Lee, W.; Nielsch, K.; Gösele, U. *Nanotechnology* **2007**, *18*, 475713.
(23) Chu, S.-Z.; Wad, K.; Inoue, S.; Isogai, M.; Yasumori, A. *Adv. Mater.* **2005**, *17*, 2115.
(24) Zhao, S.; Chan, K.; Yelon, A.; Veres, T. *Adv. Mater.* **2007**, *19*, 3004.
(25) Murphy, J. F.; Michelson, C. E. *Anodizing aluminum proceedings*; Aluminum development association: Nottingham, England, 1961; p 83.

(26) Takahashi, H.; Nagayama, M.; Akahori, H.; Kitahara, A. *J. Electron. Microsc.* **1973**, *22*, 149.

(27) Rasmussen, J. *Plat. Surf. Finish.* **2001**, *88*, 42.

(28) Li, Y.; Zheng, M.; Ma, L.; Shen, W. *Nanotechnology* **2006**, *17*, 5105.

(29) Ebihara, K.; Takahashi, H.; Nagayama, M. *J. Met. Finish. Soc. Jpn.* **1983**, *34*, 548.

(30) Keller, F.; Hunter, M. S.; Robinson, D. L. *J. Electrochem. Soc.* **1953**, *100*, 411.

(31) O'Sullivan, J. P.; Wood, G. C. *Proc. R. Soc. London, Ser. A* **1970**, *317*, 511.

(32) Li, A. P.; Müller, F.; Birner, A.; Nielsch, K.; Gösele, U. *J. Appl. Phys.* **1998**, *84*, 6023.

(33) Vrublevsky, I.; Parkoun, V.; Sokol, V.; Schrekenbach, J.; Marx, G. *Appl. Surf. Sci.* **2004**, *222*, 215.

(34) Arrowsmith, D. J.; Clifford, A. W.; Moth, D. A. *J. Mater. Sci. Lett.* **1986**, *5*, 921.

(35) Wada, K.; Shimohira, T.; Amada, M.; Baba, N. *J. Mater. Sci.* **1986**, *21*, 3810.

(36) Rühle, M. R.; Staiger, S.; Katerbau, K. H.; Wilkens, M. *Electron microscopical contrast of small cavities in metals,* 6th European Congress on Electron Microscopy; Tal. Int. Publ. Co.: 1976; p 538.

(37) Stobbs, W. M. *J. Microsc.* **1979**, *116*, 3.

(38) Alwitt, R. S.; Dyer, C. K. *J. Electrochem. Soc.* **1982**, *129*, 711.

(39) Habazaki, H.; Konno, H.; Shimizu, K.; Nagata, S.; Skeldon, P.; Thompson, G. E. *Corros. Sci.* **2004**, *46*, 2041.

(40) Zhu, X. F.; Li, D. D.; Song, Y.; Xiao, Y. H. *Mater. Lett.* **2005**, *59*, 3160.